IOPscience iopscience.iop.org

Home Search Collections Journals About Contact us My IOPscience

Electrowetting-actuated liquid metal for RF applications

This content has been downloaded from IOPscience. Please scroll down to see the full text.

2017 J. Micromech. Microeng. 27 025010

(http://iopscience.iop.org/0960-1317/27/2/025010)

View the table of contents for this issue, or go to the journal homepage for more

Download details:

IP Address: 129.137.96.19
This content was downloaded on 10/01/2017 at 14:55

Please note that terms and conditions apply.

Reprinted From
J. Micromech. Microeng

IOP Publishing Journal of Micromechanics and Microengineering
J. Micromech. Microeng. **27** (2017) 025010 (9pp) doi:10.1088/1361-6439/aa556a

Electrowetting-actuated liquid metal for RF applications

A V Diebold[1,5], A M Watson[2], S Holcomb[1], C Tabor[2], D Mast[1,4], M D Dickey[3] and J Heikenfeld[1]

[1] Novel Devices Laboratory, School of Electronics and Computing Systems, University of Cincinnati, Cincinnati, OH 45221, USA
[2] Materials and Manufacturing Directorate, Air Force Research Laboratory, Wright Patterson Air Force Base, OH 45433, USA
[3] Department of Chemical and Biomolecular Engineering, North Carolina State University, Raleigh, NC 27695, USA
[4] Department of Physics, University of Cincinnati, Cincinnati, OH 45221, USA

E-mail: heikenjc@ucmail.uc.edu

Received 21 September 2016, revised 9 December 2016
Accepted for publication 22 December 2016
Published 9 January 2017

Abstract

Electrowetting is well-established as a fluid manipulation technique in such areas as lab-on-a-chip, visible light optics, and displays, yet has seen far less implementation in the field of radio-frequency (RF) electronics and electromagnetics. This is primarily due to a lack of appropriate materials selection and control in these devices. Low loss RF conductive fluids such as room temperature liquid metals (i.e. Hg, EGaIn, Galinstan) are by far the leading choice of active material due to their superior electrical properties but require high actuating voltages due to their inherently high surface tensions (>400 mN m^{-1}) which often lead to dielectric breakdown. While the toxicity of Hg encourages the pursuit of non-toxic alternatives such as gallium alloys, the native surface oxide formation often prohibits reliable device functionality. Additionally, traditional electrowetting architectures rely on lossy electrode materials which degrade RF transmission efficiencies and result in non-reversible material diffusion at the electrode/liquid metal contact. In this work, we report on approaches to utilize liquid metals in electrowetting on dielectric (EWOD) devices that resolve all of these challenges by judicious choice of novel electrode materials, dielectric fluid, and device architecture. A functional RF device, namely an electromagnetic polarizer, is demonstrated that can be activated on demand through EWOD and provides an average signal attenuation of 12.91 dB in the on state and 1.46 dB in the off state over the range of 8–9.2 GHz, with a switching speed of about 12 ms. These results can be further extended to other RF applications such as tunable antennas, transmission lines, and switchable metasurfaces.

Keywords: liquid metal, electrowetting, radio frequency, microfluidics, reconfigurable electronics

S Online supplementary data available from stacks.iop.org/JMM/27/025010/mmedia

(Some figures may appear in colour only in the online journal)

Reprinted From J. Micromech. Microeng

Introduction

The need to reconfigure RF electronic components is becoming increasingly important in areas ranging from free space applications such as antennas to breadboard components like transmission lines. Often these reconfigurable components are rigid and introduce significant signal loss to the system, while providing only limited tunability. For example, digitally configurable electrode array antennas require lossy semi-conducting diodes or power-limited microelectromechanical

[5] Now located at Department of Electrical and Computer Engineering, Pratt School of Engineering, Duke University, Durham, NC 27708.

 © 2017 IOP Publishing Ltd Printed in the UK

systems (MEMS) switches to achieve discrete effective length changes in radiating elements [3–6]. Others require complicated placement of parasitic elements relative to a fixed antenna structure, offering modest variation of the frequency response or radiation pattern [7, 8]. In contrast, liquid metals, such as Hg and eutectic gallium indium (EGaIn) [9], offer the potential for true continuous analog physical reconfigurability [10], physical flexibility [11, 12], and high power thresholds [13] due to their high electrical conductivities (Hg conductivity $= 1.0 \times 10^6$ S m^{-1} [14]; EGaIn conductivity $= 3.4 \times 10^6$ S m^{-1} [15]). Recent work has demonstrated effective pneumatic actuation methods for liquid metal based RF components utilizing Laplace pressure shaping [16, 17] and pressure-driven flow [18]. These techniques are limited in switching speed by additional peripherals such as pumps or syringes which are not readily integrated into device architectures. Electrochemical methods to mobilize liquid metals have also been reported such as continuous electrowetting (CEW) and electrocapillarity [19–24]. These devices eliminate the need for peripheral pneumatic controls and can operate using only several volts. However, electrochemical techniques to date are significantly limited in actuation speed and require immersion in electrically lossy electrolytic solutions, which have limited their use in RF applications.

Electrowetting has emerged as an attractive alternative for liquid metal actuation [25–28] which, in theory, can resolve many of the challenges that exist for the above approaches. Electrowetting in other applications has allowed for automated transport and mixing of biofluids [29], tuning of microprism arrays [30], adjusting variable-focus lenses [31], and altering reflective displays [32]. The phenomenon relies on variation of droplet contact angle by electromechanical force, resulting in a variety of fundamental operations [33].

There are two prominent obstacles in utilizing electrowetting to reconfigure liquid metals for RF applications. Firstly, there is a prohibitively large contact angle change (>90°) required to cause reversible capillary wetting/dewetting of a droplet into and out of an open-ended channel or capillary. To date, electrowetting of liquid metal has been reported to only evoke modest changes in shape and contact angle of a small drop of metal in a few limited switch based applications. Feinerman *et al* have reported two types of micromirrors which function by varying the contact angle of a sessile drop of Hg [26, 27]. In [34], the authors present a frequency reconfigurable antenna, where frequency tuning results from the change in capacitive loading as the wetting state of a droplet of Hg is varied electrostatically. A similar method drives the frequency sweep in an RF MEMS resonator in [35]. Finally, Kim *et al* have made significant contributions to the development and optimization of liquid metal switches based on electrowetting of Hg [28, 36]. The contact angle change required for more significant fluid mobilization and RF tuning is prohibited by the high surface tensions of liquid metals (>400 mN m^{-1} [1, 2]) which results in excessive voltage requirements (>1 kV) to achieve large angle changes that are often beyond or near the breakdown limit of practical dielectric films.

Further complicating matters, when attempting to use non-toxic alternatives to mercury such as gallium liquid metal alloys (GaLMAs) (EGaIn and Galinstan), rapid gallium oxide formation occurs on the metal surface which renders electrowetting inoperable due to the highly adhesive and viscoelastic properties of the oxide [9, 10, 37]. Simply using an inert gas is impractical as even <1 ppm oxygen levels over time will cause some degree of oxide formation [38, 39]. Kim *et al* in [40] have performed extensive characterization of Galinstan in a nitrogen glove box held below 0.5 ppm oxygen, concluding that true liquid behavior is attained at levels below 1 ppm oxygen. Reversible electrowetting was successfully demonstrated in that report. However, these levels of O_2 concentration are incredibly difficult to maintain in a device. An acidic vapor background for chemical removal [10, 41] of the oxide skin is also unusable with electrowetting, because an aqueous annulus forms near the electrowetting contact line [42], which in our experience will electrowet *instead* of the liquid metal (see supplemental information (stacks.iop.org/JMM/27/025010/mmedia)).

We report here fully integrated devices that utilize several key novel approaches to resolve these challenges for liquid metal electrowetting, and furthermore, we demonstrate a functional RF device in the form of an electromagnetic polarizer that can be actuated on demand. The enabling innovations include a geometric microchannel design which greatly reduces the required contact angle range needed for actuation, the use of an RF transparent conducting polymer as the contacting electrode, and the use of a novel acidic and electrically insulating oil that eliminates the oxide-induced limitations associated with utilizing non-toxic GaLMAs instead of mercury in these devices [43]. Material optimization then enables the demonstration of a switchable wire-grid polarizer, which provides an average signal attenuation of 12.91 dB in the on state and 1.46 dB in the off state, over the range of 8–9.2 GHz, with a switching speed of 12 ms.

Reprinted From
J. Micromech. Microeng

Materials and fabrication of test devices

Electrowetting characterization

Mercury and EGaIn were used as purchased (Aldrich, Hg, >99.99% trace metals basis; Aldrich, Gallium-Indium eutectic, >99.99% trace metals basis). Contact angle characterization with voltage was performed on glass substrates coated with In_2O_3:SnO_2 (Kaivo, <10 Ω/square), 3.8 μm of chemical vapor deposited Parylene C (Specialty Coating Systems, $\varepsilon_r = 3.1$), and a top monolayer of hydrophobic FluoroPel PFC 1601V (Cytonix). The monolayer was created using a surface grafting technique, described elsewhere [44]. Electrowetting of mercury was performed in Dow Corning® OS-20 silicone oil purchased from Krayden. Electrowetting of EGaIn was performed in an open bath of specially formulated acidic silicone oil. Synthesis and characterization of this oil has been performed in detail by our group. More details on the oil are provided in the experimental results section and

are reported elsewhere [43]. Contact angle change was driven by a 1 kHz square wave voltage. Contact angle measurements were performed using a VCA Optima contact angle analysis system.

Polarizer device demonstration

The polarizer fabrication consists of a bottom plate supporting channels aligned with patterned bottom electrodes coated with a thin dielectric. The top plate is coated with an electrode material in addition to thin ridges patterned perpendicular to the bottom channels (figure 1).

The bottom plate of the polarizer was fabricated by first spin-coating positive photoresist (Microposit S1818) onto a glass slide, then patterning with 500 mJ cm^{-2} of i-line energy in the negative of the electrode pattern. The electrode pattern consists of a series of parallel stripes, 475 μm in width, pitch 1.68 mm center to center, connected by a single contact pad at the bottom. A thin layer (<100 nm) of gold was then sputtered onto the glass/photoresist structure and patterned using the lift-off technique.

Next, channels were formed on the bottom plate by spin-coating 72.3% solids SU-8 3000 series (Microchem) negative photoresist at 1800 rpm, yielding a thickness of 40 μm, followed by a soft bake at 100 °C for 15 min. Channels with width 958 μm were aligned and exposed as above, and then a post exposure bake was performed for 5 min at 100 °C. Finally, the photoresist was developed in PGMEA, and the entire structure hard baked at 180 °C for 30 min. Next, a 3.5 μm thick coating of Parylene C and monolayer of FluoroPel PFC 1601V were deposited as previously described for the electrowetting test plates.

Poly(3,4-ethylenedioxythiophene) polystyrene sulfonate (PEDOT:PSS) (Aldrich, 1.3 wt% dispersion in H_2O) was chosen for the electrode material on the top plate for reasons described below and was spun on at 2500 rpm, and then baked at 120 °C for 15 min. This was repeated twice in order to achieve the desired conductance. The sample was then heated under vacuum for 30 min at 110 °C, to remove any water absorbed by the PEDOT:PSS.

Ridges of thickness 10 μm, width 1.46 mm, and spacing 2.46 mm were patterned by spinning 50% solids SU-8 3000 series negative resist at 1000 rpm onto the cured PEDOT:PSS, then baking and patterning as described above. This structure was coated with a monolayer of FluoroPel PFC 1601V to achieve hydrophobicity while still maintaining electrical contact [45].

Polarization measurements consisted of a signal from a Hewlett-Packard 8684B Signal Generator being fed through an X-band waveguide and emitted by a Budd Stanley E-plane sectoral horn antenna (X4100-611). Transmitting and receiving antennas were placed a distance of 1.45 cm apart, and the polarizer device placed directly between them (≈ 0.7 cm from each antenna). The antennas measure 27.6 mm in the direction of the *E*-field and 22.8 mm in the H-plane (629.28 mm^2), whereas the active area of the polarizer measures 1760 mm^2. Signal amplitude values were obtained using an IFR AN930 spectrum analyzer. High speed photos were taken using a Fastec Troubleshooter camera.

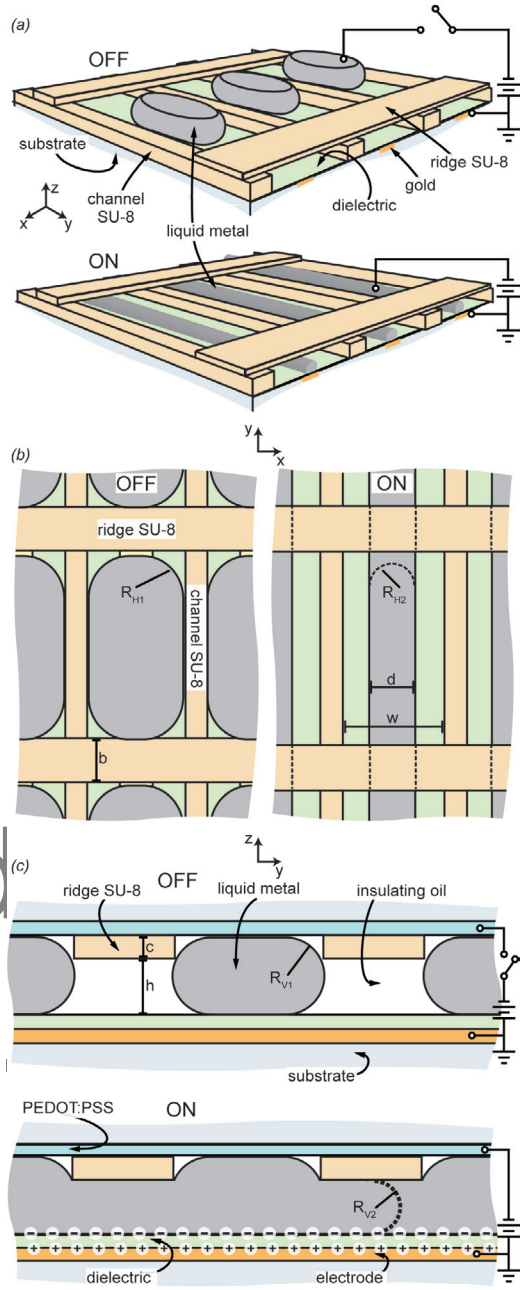


Figure 1. Device diagrams and relevant dimensions for switchable polarizer. (a) Perspective view. (b) Top view. (c) Side view.

Theory/liquid metal electrowetting device design

Electrowetting involves an apparent change in contact angle of an electrically conductive fluid under an applied voltage [46]. The Young–Lippmann equation relates interfacial surface tensions to the equilibrium contact angle of a sessile drop:

$$\cos\theta_V = \cos\theta_Y + \frac{\varepsilon_0\varepsilon_r V^2}{2\gamma_{ci}t} \quad (1)$$

Reprinted from J Micromech Microeng

where ε_0 is the permittivity of free space, ε_r is the relative permittivity of the dielectric used, γ_{ci} is the interfacial surface tension between the conducting fluid and the insulating ambient, t is the thickness of the dielectric coating, V is the applied voltage between the bottom and top electrode, and θ_Y is the resting Young's contact angle under zero applied potential.

As the intent of this work is to change the shape of a liquid metal droplet, we choose to model our problem in terms of droplet pressure, which has explicit dependence on droplet shape. Laplace pressure Δp, the pressure difference across the boundary of a liquid, is related to the shape of a droplet by the Young–Laplace equation [46]:

$$\Delta p = \gamma_{ci}\left(\frac{1}{R_1}+\frac{1}{R_2}\right) \tag{2}$$

where R_1 and R_2 are the principal radii of curvature of the droplet. We see that the high surface tension of the liquid metal, γ_{ci}, results in high values for the droplet Laplace pressure.

In electrowetting, the electrostatic driving pressure on a conducting droplet in a channel of height $(h+c)$ may be expressed as [47, 48]:

$$\Delta p_e = \frac{\varepsilon_0\varepsilon_r V^2}{2(h+c)t}. \tag{3}$$

Transitions between droplet shape configurations may thus be achieved by supplying adequate electrostatic pressure. That is, the supplied electrostatic pressure must exceed the difference between some initial state, Δp_1, and the desired final state Δp_2.

$$\Delta p_2 - \Delta p_1 < \Delta p_e. \tag{4}$$

Our goal is to minimize this required electrostatic pressure through proper device design.

In the case of the liquid metal polarizer, the desired final shape of each droplet (figure 1) is a strip of width d (radius of curvature $R_{H2} = d/2$, dictated by electrode width) and height h (radius of curvature $R_{V2} \approx h/2$, dictated by channel height). Representation of R_{V2} as half of the channel height is a reasonable assumption for EGaIn given its very high surface tension which allows use of the approximation of a 180° Young's angle on the fluoropolymer surface.

In order to minimize the electrostatic pressure required to achieve this state, we place our droplet in an initial state Δp_1 as close to its final state Δp_2 as to still allow proper device functionality. This is achieved by confining the droplet in a channel of width w (radius of curvature $R_{H1} = w/2$) which is larger than the electrode width d only by the amount required by volume conservation. The droplet is confined vertically to a height larger than that achieved in its final state by a small amount c (radius of curvature $R_{V1} \approx (h+c)/2$). The result of this confinement is twofold. First, it reduces the pressure difference between the two states which must be supplied electrostatically, as discussed above. Second, it enhances the electrostatic pressure contribution according to equation (3) by substantially reducing the height of the droplet.

Additional channel height in the amount c is enabled by patterning ridges of thickness c perpendicular to the channels of height h. The resulting variation in channel height ensures that droplets preferentially dewet into areas of larger channel height, i.e. lower Laplace pressure, upon removal of voltage. Contributions to required voltage due to this variation in channel height were minimized by making dewetting ridges wide and thin, since dewetting reliability increases both with ridge width and thickness, but electrostatic pressure requirements increase only with ridge thickness.

Thus, each droplet wets as desired (figure 1) once the supplied electrostatic pressure exceeds the pressure difference between the initial array configuration and the final, merged state. According to equation (4), this condition is expressed as:

$$\frac{2\gamma_{ci}}{h}+\frac{2\gamma_{ci}}{d}-\frac{2\gamma_{ci}}{h+c}-\frac{2\gamma_{ci}}{w} < \frac{\varepsilon_0\varepsilon_r V^2}{2(h+c)t}. \tag{5}$$

We see that because the liquid metal is confined it is presented with a starting Laplace pressure which aids our goal of electromechanically changing its shape into features such as wires. Ohta *et al* in [49] interpret this mechanism with a surface energy approach, where confinement effectively biases the droplet such that minor changes in electrostatic energy effect large in-plane deformations. As noted in the introduction, electrowetting a sessile liquid metal droplet into a capillary or open-face rectangular channel would require a much larger change in droplet pressure, which in our experience is often prohibitive in terms of voltage and dielectric reliability (figure 5).

The dimensions employed in the polarizer design indicate that the onset of diffraction occurs at a frequency of 89 GHz for the wire-grid polarizer [50], well above the frequencies tested here.

Reprinted From
J. Micromech. Microeng

Experimental results

A device was fabricated according to the above dimensions with mercury as the conducting fluid in a silicone oil bath and was verified to function as predicted from the above equations. Operation of the liquid metal polarizer device was first characterized by measuring droplet edge velocity in an Hg-loaded device using a standard ITO electrode, captured by a high speed camera. Figure 2 plots the length change of Hg as a function of time. For these plots a voltage of 330 V was utilized, corresponding to an expected minimum contact angle of 90° based on the Young–Lippmann equation. A maximum length change of about 78% is observed over 12 ms, corresponding to the switch on time. A similar response is observed in the case of dewetting, or switching off. This implies an average wetting speed of 10.3 cm s^{-1}.

Before the device could be tested as a wire-grid polarizer, a replacement for the In_2O_3:SnO_2 (<10 Ω/square) was needed because of excessive transmission loss in the GHz frequencies. Figure 3 illustrates the transmission profiles for various possible electrode materials. A thin layer of sputtered gold (<100 nm) was employed for the bottom electrodes due to its low attenuation and ease of patterning. PEDOT:PSS conductive polymer was used as the top electrode due to its similarly

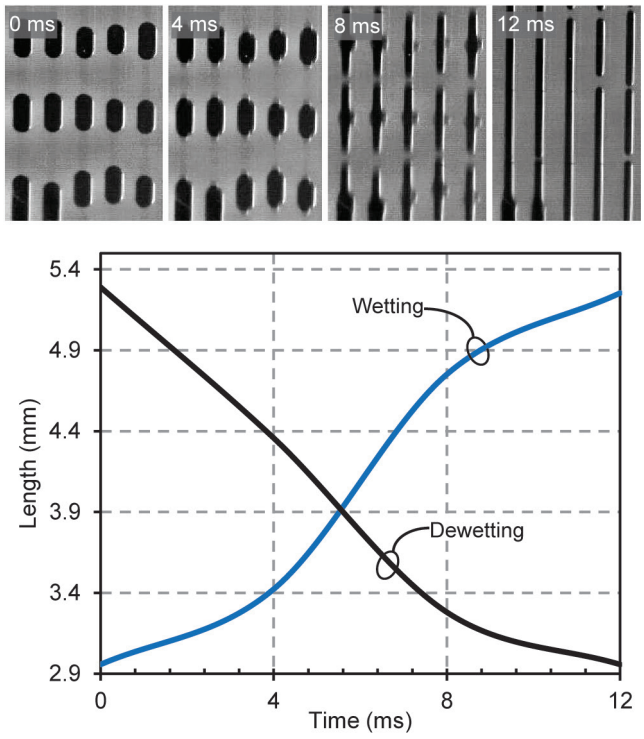


Figure 2. Wetting and dewetting speeds in polarizer.

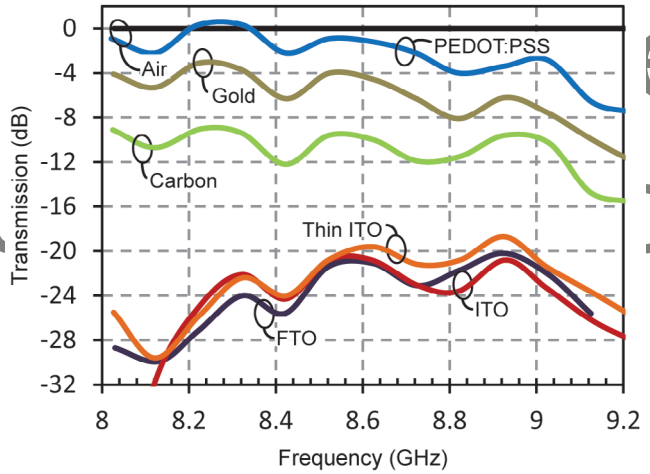


Figure 3. Signal transmission for various electrode materials including fluorine doped tin oxide (FTO) and indium tin oxide (ITO).

low signal attenuation as well as its availability in dispersion form and potential application in flexible electronics. Most importantly, compatibility with EGaIn and Hg requires that the bare top electrode be of a non-alloying material. Conductive polymers, such as PEDOT:PSS, are a natural candidate in this regard, although their RF properties have not been thoroughly studied to date.

After substituting the above materials into the device, polarizer attenuation for the Hg device was measured in the X-band using horn antennas. The device was actuated with 330 V AC, using a frequency of 100 Hz, in order to allow for proper capacitive discharge while still preventing dielectric charging that results from the electrowetting process [51].

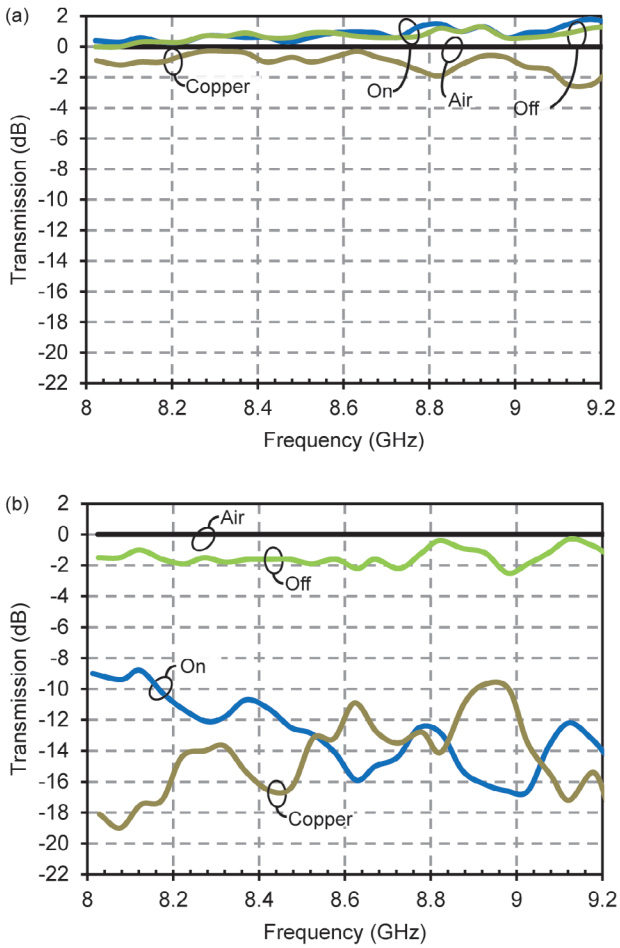


Figure 4. Transmission results for device on and off, with the liquid metal wires (a) perpendicular and (b) parallel to the electric field polarization.

RF transmission measurements are depicted in figure 4 for the polarizer in the off (4A) and on (4B) states, with liquid metal 'wires' oriented both perpendicular and parallel to the polarization of the electric field. When aligned perpendicular to the electric field polarization, there was no observed signal attenuation, which indicates that losses due to reflection are negligible. In this orientation, transmission greater than that of air may be due to near field effects, or to measurement error. When aligned parallel to the electric field polarization, the device exhibited an average attenuation of 12.91 dB in the on state and 1.464 dB in the off state over the range 8–9.2 GHz. As comparison, a patterned copper polarizer of similar dimensions offered an average signal attenuation of 14.51 dB over the same range.

An important consideration for RF liquid electronics, is the choice of conducting fluid. As mentioned previously, the use of Hg is highly contentious due to toxicity concerns and potential loss of material over time due to the high vapor pressure. The substitution of GaLMAs for mercury as a non-toxic, near-0 vapor pressure alternative has seen recent attention in the literature, but presents the new concern of surface oxide formation and its effects on electrowetting actuation. Here, we demonstrate for the first time the electrowetting actuation of a

common GaLMA fluid, namely EGaIn, in a device architecture nearly identical to the wire-grid polarizer presented above and enabled by the use of a novel acidic silicone oil. Oxidized EGaIn droplets are viscoelastic, so that arbitrary shapes attained by any means of actuation are maintained once the stimulus (e.g. voltage) is removed [10] (see figure 5). Further complications arise from the highly adhesive quality of the gallium oxide skin, as well as the consequent oxide residue which irreparably fouls devices [37, 52]. Achieving reversible and reliable electrowetting of EGaIn thus requires oxide-free droplets. In our work, this is achieved through the use of an electrically insulating acidic silicone oil, as presented in [43].

The electrowetting response data shown in figure 5 displays the dependence of the contact angle on voltage as a function of varying HCl concentrations in the silicone oil [43]. The black curve corresponds to the theoretical response predicted by the electrowetting equation, using a surface tension of 445 mN m^{-1} [1].

To fabricate the acidic oil, HCl was added to Ar-purged silicone oil until the oil is saturated with HCl (maximum molarity of 1.5 M, 6.28 wt% HCl [43]). This HCl-saturated oil was then diluted with regular oil. Therefore here and in figure 5 we will describe oil concentrations as the volume % of HCl-saturated oil blended with regular oil (e.g. 100% is HCl-saturated oil).

Our tests were performed in a 1 cm-thick acidic oil bath open to air, so that after the initial oxygen-free oil is dispensed, the diffusion rate of oxygen through the oil determines the concentration of oxygen in the oil.

The effects of silicone oil with low HCl concentrations on enabling EGaIn electrowetting in ambient environments are presented in figure 5(a). The 0% curve illustrates the contact angle change of an EGaIn droplet in silicone oil with no HCl content. Though dissolved oxygen content was minimized by purging the oil with Ar, the droplet was observed to be oxidized immediately after being dispensed. This was evidenced by obvious deformation of the droplet from a spherical shape. Oxidation was confirmed by the extreme contact angle hysteresis observed, which derives from the viscoelastic and adhesive characteristics of oxidized EGaIn. This result highlights the irreversibility of electrowetting with oxidized EGaIn. Fluctuations in this curve are due to gradual shape change as oxidation progresses. The curves corresponding to 3% and 6% HCl content show good agreement with theory, as well as no observed hysteresis, indicating that oxide is minimized by continual reaction of HCl such that the droplet regains elasticity.

At higher HCl concentrations (figure 5(b)), the contact angle response of EGaIn becomes less consistent, and at higher voltages (>200 V) the droplet vibrates/oscillates visibly, so that accurate contact angle values become difficult to retrieve. Measurements for the 30% and 60% cases terminate at 250 V due to motion of the droplet becoming so significant that the droplet leaves the probe. Similar behavior has been reported in [25] and observed in our lab for the case of Hg. At significantly higher concentrations, i.e. 80% and 100%, total contact angle change from 0–300 V is drastically reduced. This behavior may possibly be attributed to screening effects due to charging of the oil and dielectric, as well as water

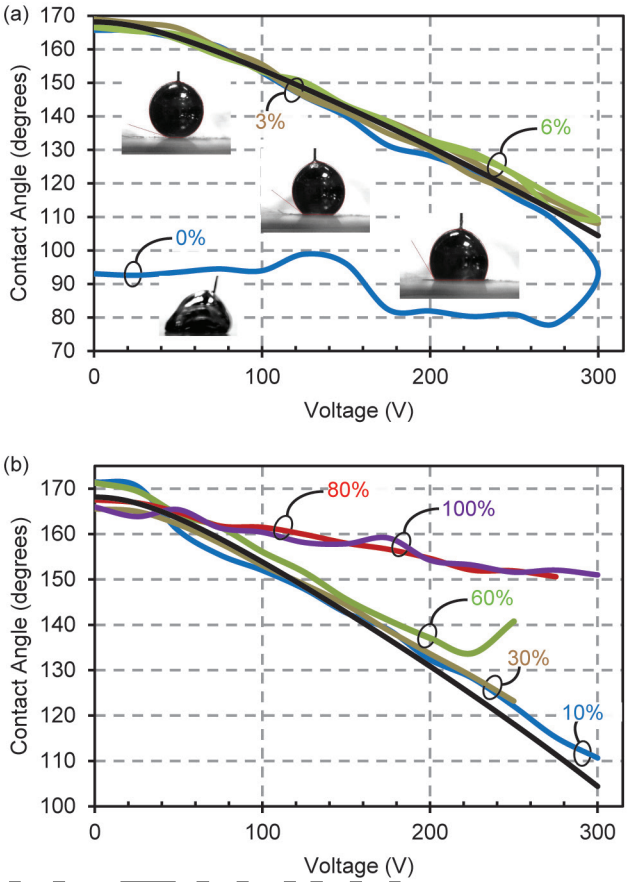


Figure 5. Contact angle change of EGaIn versus AC voltage using a 1 kHz square wave in acidic oil with (a) low concentrations of HCl and (b) high concentrations of HCl. The percentage values refer to the volume % of HCl-saturated oil blended with regular oil (see text).

generation which is a product of the reaction of HCl with gallium oxide species [41]. The exact mechanism responsible has not been definitively investigated in this work.

These high concentrations represent an upper bound for the range of practical concentrations when electrical insulation is required at such voltages. It should be noted that we fully expect that in a sealed system, much lower concentrations of HCl in the oil would be permitted.

Device actuation was then tested with EGaIn in a low-oxygen glovebox held below 1 ppm oxygen, which has been reported to increase the longevity of oxide-free GaLMAs [40]. In our observation, in a glove box at these oxygen levels, the droplets oxidized enough to prevent device operation within minutes when no HCl oil was utilized. Indeed, others report more stringent environmental requirements for oxide prevention, such as ultrahigh (10^{-9} Torr) vacuum systems, with oxidation rates steadily increasing at higher pressures [38, 39]. We thus concluded that optimal device performance would be achieved by assembling the device in the glove box in concert with the use of acidic oil for active oxide removal. Slight modifications to the wire grid polarizer were made to enable this assembly, as detailed in the supplemental information.

Photos of the fully functioning EGaIn wire-grid polarizer device are provided in figure 6, with prominent device features indicated by dotted white lines. One of the challenges

Reprinted from
J. Micromech. Microeng

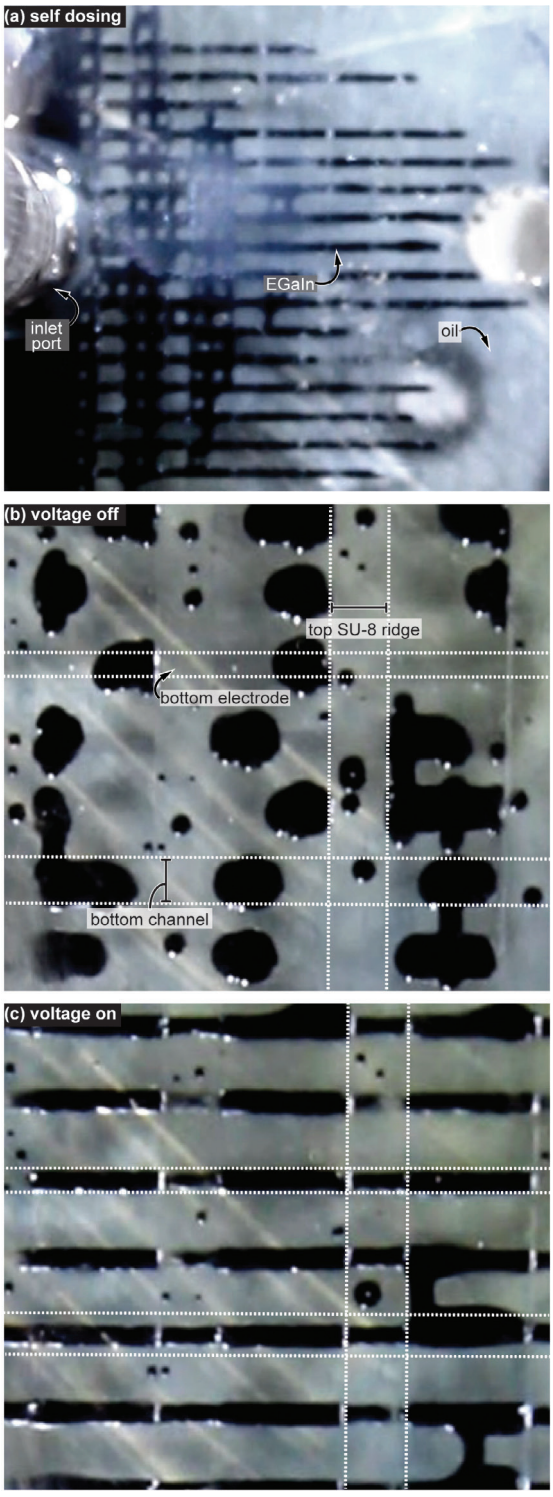


Figure 6. Photos of operating device, including (a) initial self-loading, (b) with voltage off, and (c) with voltage on.

with arrayed electrowetting devices, such as a wire-grid polarizer, is dosing discrete volumes of fluids. In our previous work, we have developed self-assembly dosing techniques for electrowetting [53] and electrofluidic displays [32, 54]. Here, we again demonstrate a self-assembly approach to initially dose the EGaIn into the device. As shown in figure 6(a), self-assembled dosing of the device is enabled by the effect of the electrowetting electrodes in combination with a pressurized reservoir at the bottom of the device which spans all of the stripe electrodes. Simply, the liquid metal is pulled into the channels by electrowetting (figure 6(a)), and when the voltage is removed, is deterministically split into discrete droplets by the greater Laplace pressure imparted by the top SU-8 ridge (figure 6(b)). The transition between the electrowetted wire-grid polarizer state of figure 6(c) and the discrete droplet array of figure 6(b) was reversible and fast (~12 ms, figure 3)—the same speed demonstrated for Hg in figure 2.

Discussion

If the mechanism demonstrated in this paper is to be widely employed, several remaining challenges should be mentioned. Some improvements can be expected if one were to shrink device dimensions. As switching speed is determined partially by ridge width, a uniform scaling of device dimensions would result in an increased switching speed.

Variations in droplet size and line width can be seen in the device photos and supplemental video. Such effects are a result of imprecise device loading techniques (syringe injection, by hand) and of device modifications (discussed in the supplemental information). For example, the replacement of channel walls with discrete posts maximizes the exposure to the acidic oil, but also reduces the confinement of the droplets. These and other issues are likely resolvable with future optimization of the device design and assembly techniques.

Our demonstration of device functionality has not ruled out partial oxidation of the droplets, again leaving room for future improvement. In fact, due to the dynamic nature of oxide formation and etching, an acid concentration dependence is expected, and can be seen in the contact angle behavior illustrated in figure 5.

Though environmental temperature may affect device performance, such effects were not considered in this work, other than that obviously the operating temperature was above the melting point of the liquid metals. Simply, all tests were performed at room temperature.

Regarding device design, sputtered gold was used as the bottom electrodes due to its ease of patterning. The 1.464 dB signal loss in the parallel, off state is most likely caused by this gold layer. Substitution of patterned PEDOT:PSS would adequately reduce these off-state losses. Methods of patterning PEDOT:PSS have been demonstrated in [55, 56].

To promote device longevity with GaLMAs materials, devices should be assembled with proper hermetic sealing in order to prevent acid evaporation, oxygen diffusion and the resulting oxidation of EGaIn. We have found that certain acids react with EGaIn in undesirable ways [43], such that lower concentrations are preferred, or else alternative formulations must be used to achieve longer device lifetimes. Also, lower acid concentrations will decrease the amount of acid which partitions into the dielectric materials, which is preferred from an electrical reliability perspective.

Downloaded From J. Micromech. Microeng.

Conclusions

Reliable electrowetting of liquid metal for RF applications has been demonstrated in this work following the investigation of an improved device architecture and several enabling materials. A newly-developed acidic oil was used to enable EGaIn mobility due to its ability to remain electrically insulating while mitigating detrimental surface oxide effects. Further, the use of a low loss conducting polymer, PEDOT:PSS, was used as the electrode that electrically contacts the liquid metals without chemically alloying with them. A switchable polarizer utilizing electrowetting has been demonstrated which offers an average signal attenuation of 12.91 dB over the frequency range 8–9.2 GHz, with switching speeds of about 12 ms. This method lays the groundwork for future devices allowing arbitrary physical reconfiguration of liquid metal components for RF applications, bridging the gap between two areas of vast potential in the field of microfluidics. The approach has significant promise in areas where increased efficiency requires active components to be segregated from the actuation components, such as frequency-shifting antennas, electronic switches, variable impedance transmission lines, and reconfigurable metamaterials.

Acknowledgments

We are grateful for valuable discussion with Dr Michael Brothers, Dr Alex Schultz and Dr Phillip Schultz of Okeanos Technologies, as well as Dr Brad Cumby at the Air Force Research Laboratory.

Reprinted from J. Micromech. Microeng

References

[1] Xu Q, Oudalov N, Guo Q, Jaeger H M and Brown E 2012 Effect of oxidation on the mechanical properties of liquid gallium and eutectic gallium–indium *Phys. Fluids* **24** 63101
[2] Aqra F and Ayyad A 2011 Theoretical calculations of the surface tension of liquid transition metals *Metall. Mater. Trans.* B **42** 5–8
[3] Roscoe D J, Shafai L, Ittipiboon A, Cuhaci M and Douville R 1993 Tunable dipole antennas *Proc. IEEE* 672–5
[4] Piazza D, Kirsch N, Forenza A, Heath R and Dandekar K 2011 Design and evaluation of a reconfigurable antenna array for MIMO systems *IEEE Trans. Antennas Propag.* **56** 869–81
[5] Fries M K, Grani M and Vahldieck R 2003 A reconfigurable slot antenna with switchable polarization *IEEE Microw. Wirel. Compon. Lett.* **13** 490–2
[6] Pringle L N, Harms P H, Blalock S P, Kiesel G N, Kuster E J, Friederich P G, Prado R J, Morris J M and Smith G S 2004 A reconfigurable aperture antenna based on switched links between electrically small metallic patches *IEEE Trans. Antennas Propag.* **52** 1434–45
[7] Zhang S, Huff G H, Feng J and Bernhard J T 2004 A pattern reconfigurable microstrip parasitic array *IEEE Trans. Antennas Propag.* **52** 2773–6
[8] Harrington R 1978 Reactively controlled directive arrays *IEEE Trans. Antennas Propag.* **26** 390–5
[9] Dickey M D 2014 Emerging applications of liquid metals featuring surface oxides *Appl. Mater. Interfaces* **6** 18369–79
[10] Dickey M D, Chiechi R C, Larsen R J, Weiss E A, Weitz D A and Whitesides G M 2008 Eutectic gallium–indium (EGaIn): a liquid metal alloy for the formation of stable structures in microchannels at room temperature *Adv. Funct. Mater.* **18** 1097–104
[11] Hayes G J, So J-H, Qusba A, Dickey M D and Lazzi G 2012 Flexible liquid metal alloy (EGaIn) microstrip patch antenna *IEEE Trans. Antennas Propag.* **60** 2151–6
[12] Zhu S, So J H, Mays R, Desai S, Barnes W R, Pourdeyhimi B and Dickey M D 2013 Ultrastretchable fibers with metallic conductivity using a liquid metal alloy core *Adv. Funct. Mater.* **23** 2308–14
[13] So J H, Thelen J, Qusba A, Hayes G J, Lazzi G and Dickey M D 2009 Reversibly deformable and mechanically tunable fluidic antennas *Adv. Funct. Mater.* **19** 3632–7
[14] Surmann P and Zeyat H 2005 Voltammetric analysis using a self-renewable non-mercury electrode *Anal. Bioanal. Chem.* **383** 1009–13
[15] Zrnic D and Swatik D S 1969 On the resistivity and surface tension of the eutectic alloy of gallium and indium *J. Less-Common Met.* **18** 67–8
[16] Cumby B L, Hayes G J, Dickey M D, Justice R S, Tabor C E and Heikenfeld J C 2012 Reconfigurable liquid metal circuits by Laplace pressure shaping *Appl. Phys. Lett.* **101** 174102
[17] Cumby B, Heikenfeld J, Mast D, Tabor C and Dickey M 2015 Robust pressure-actuated liquid metal devices showing reconfigurable electromagnetic effects at GHz frequencies *IEEE Trans. Microw. Theory Tech.* **63** 3122–30
[18] Wang J, Liu S, Vardeny Z V and Nahata A 2012 Liquid metal-based plasmonics *Opt. Express* **20** 2346–53
[19] Eaker C B and Dickey M D 2016 Liquid metal actuation by electrical control of interfacial tension *Appl. Phys. Rev.* **3** 31103
[20] Wang M, Trlica C, Khan M R, Dickey M D and Adams J J 2015 A reconfigurable liquid metal antenna driven by electrochemically controlled capillarity *J. Appl. Phys.* **117** 194901
[21] Khan M R, Eaker C B, Bowden E F and Dickey M D 2014 Giant and switchable surface activity of liquid metal via surface oxidation *Proc. Natl Acad. Sci.* **111** 14047–51
[22] Lee J and Kim C J 2000 Surface-tension-driven microactuation based on continuous electrowetting *J. Microelectromech. Syst.* **9** 171–80
[23] Gough R C, Morishita A M, Dang J H, Hu W, Shiroma W A and Ohta A T 2014 Continuous electrowetting of non-toxic liquid metal for RF applications *IEEE Access* **2** 874–82
[24] Khan M R, Trlica C, So J, Valeri M and Dickey M D 2014 Influence of water on the interfacial behavior of gallium liquid metal alloys *ACS Appl. Mater. Interfaces* **6** 22467–73
[25] Wan Z, Zeng H and Feinerman A 2007 Reversible electrowetting of liquid–metal droplet *J. Fluids Eng.* **129** 388–94
[26] Zeng H, Feinerman A D, Wan Z and Patel P R 2005 Piston-motion micromirror based on electrowetting of liquid metals *J. Microelectromech. Syst.* **14** 285–94
[27] Wan Z, Zeng H and Feinerman A 2006 Area-tunable micromirror based on electrowetting actuation of liquid–metal droplets *Appl. Phys. Lett.* **89** 201107
[28] Sen P and Kim C-J 2009 A fast liquid–metal droplet microswitch using EWOD-driven contact-line sliding *J. Microelectromech. Syst.* **18** 174–85
[29] Hua Z, Rouse J L, Eckhardt A E, Srinivasan V, Pamula V K, Schell W A, Benton J L, Mitchell T G and Pollack M G 2010 Multiplexed real-time polymerase chain reaction on a digital microfluidic platform *Anal. Chem.* **82** 2310–6
[30] Smith N R, Abeysinghe D C, Haus J W and Heikenfeld J 2006 Agile wide-angle beam steering with electrowetting microprisms *Opt. Express* **14** 6557–63

[31] Kuiper S and Hendriks B H W 2004 Variable-focus liquid lens for miniature cameras *Appl. Phys. Lett.* **85** 1128–30
[32] Heikenfeld J, Zhou K, Kreit E, Raj B, Yang S, Sun B, Milarcik A, Clapp L and Schwartz R 2009 Electrofluidic displays using Young–Laplace transposition of brilliant pigment dispersions *Nat. Photon.* **3** 292–6
[33] Cho S K, Moon H and Kim C J 2003 Creating, transporting, cutting, and merging liquid droplets by electrowetting-based actuation for digital microfluidic circuits *J. Microelectromech. Syst.* **12** 70–80
[34] Damgaci Y and Cetiner B A 2013 A frequency reconfigurable antenna based on digital microfluidics *Lab Chip* **13** 2883–7
[35] Irshad W and Peroulis D 2011 A 12–18 GHz electrostatically tunable liquid metal RF MEMS resonator with quality factor of 1400–1840 *2011 IEEE MTT-S Int. Microwave Symp. Digest (MTT)* vol 2 pp 3–6
[36] Kim J, Shen W, Latorre L and Kim C-J 2002 A micromechanical switch with electrostatically driven liquid–metal droplet *Sensors Actuators* A **97–8** 672–9
[37] Doudrick K, Liu S, Mutunga E M, Klein K L, Damle V, Varanasi K K and Rykaczewski K 2014 Different shades of oxide: from nanoscale wetting mechanisms to contact printing of gallium-based liquid metals *Langmuir* **30** 6867–77
[38] Chabala J M 1992 Oxide-growth kinetics and fractal-like patterning across liquid gallium surfaces *Phys. Rev.* B **46** 11346
[39] Su C Y, Skeath P R, Lindau I and Spicer W E 1982 Photoemission studies of room-temperature oxidized Ga surfaces *Surf. Sci.* **118** 248–56
[40] Liu T, Sen P and Kim C J 2012 Characterization of nontoxic liquid-metal alloy galinstan for applications in microdevices *J. Microelectromech. Syst.* **21** 443–50
[41] Nekrasov S Y, Migdisov A A, Williams-Jones A E and Bychkov A Y 2013 An experimental study of the solubility of Gallium(III) oxide in HCl-bearing water vapour *Geochim. Cosmochim. Acta* **119** 137–48
[42] Kim D, Thissen P, Viner G, Lee D, Choi W, Chabal Y J and Lee J B 2013 Recovery of nonwetting characteristics by surface modification of gallium-based liquid metal droplets using hydrochloric acid vapor *Appl. Mater. Interfaces* **5** 179–85
[43] Holcomb S, Brothers M, Diebold A, Thatcher W, Mast D, Tabor C and Heikenfeld J 2016 Oxide-free actuation of gallium liquid metal alloys enabled by novel acidified siloxane oils *Langmuir* **32** 12656–63
[44] Berry S, Fedynyshyn T, Parameswaran L and Cabral A 2012 Reversible electrowetting on dual-scale-patterned corrugated microstructured surfaces *J. Microelectromech. Syst.* **21** 1261–71
[45] Kreit E, Mognetti B M, Yeomans J M and Heikenfeld J 2011 Partial-post laplace barriers for virtual confinement, stable displacement, and $>5\,\mathrm{cm\ s^{-1}}$ electrowetting transport *Lab Chip* **11** 4221–7
[46] Mugele F and Baret J-C 2005 Electrowetting: from basics to applications *J. Phys.: Condens. Matter* **17** R705–74
[47] Lee J, Moon H, Fowler J, Schoellhammer T and Kim C-J 2002 Electrowetting and electrowetting-on-dielectric for microscale liquid handling *Sensors Actuators* A **95** 259–68
[48] Fair R B 2007 Digital microfluidics: is a true lab-on-a-chip possible? *Microfluid. Nanofluid.* **3** 161–8
[49] Gough R C, Morishita A M, Dang J H, Moorefield M R, Shiroma W A and Ohta A T 2015 Rapid electrocapillary deformation of liquid metal with reversible shape retention *Micro Nano Syst. Lett.* **3** 1–9
[50] Bass M 1995 *Handbook of Optics* vol II (New York: McGraw-Hill)
[51] Thomas D, Audry M-C, Thibaut R-M, Kleimann P, Chassagneux F, Maillard M and Brioude A 2015 Charge injection in dielectric films during electrowetting actuation under direct current voltage *Thin Solid Films* **590** 224–9
[52] Koo C, LeBlanc B E, Kelley M, Fitzgerald H E, Huff G H and Han A 2014 Manipulating liquid metal droplets in microfluidic channels with minimized skin residues toward tunable RF applications *J. Microelectromech. Syst.* **24** 1069–76
[53] Sun B and Heikenfeld J 2008 Observation and optical implications of oil dewetting patterns in electrowetting displays *J. Micromech. Microeng.* **18** 25027
[54] Yang S, Zhou K, Kreit E and Heikenfeld J C 2010 High reflectivity electrofluidic pixels with zero-power grayscale operation *Appl. Phys. Lett.* **97** 143501
[55] Li D and Guo L J 2006 Micron-scale organic thin film transistors with conducting polymer electrodes patterned by polymer inking and stamping *Appl. Phys. Lett.* **88** 63513
[56] Xiao S 2011 Picosecond laser direct patterning of poly(3,4-ethylene dioxythiophene)-poly(styrene sulfonate) (PEDOT:PSS) thin films *J. Laser Micro/Nanoeng.* **6** 249–54

Reprinted from
J. Micromech. Microeng